J|A|C|S
ARTICLES
Published on Web 03/12/2005

Molecular Dynamics Simulation Study on a Monolayer of Half [2]Rotaxane Self-Assembled on Au(111)

Yun Hee Jang, Seung Soon Jang, and William A. Goddard, III*

Contribution from the Materials and Process Simulation Center, Beckman Institute (139-74), California Institute of Technology, Pasadena, California 91125

Received August 30, 2004; E-mail: wag@wag.caltech.edu

Abstract: The self-assembled monolayer (SAM) structure of the tetrathiafulvalene-side half of the Stoddart−Heath type [2]rotaxane on Au(111) surface was investigated using molecular dynamics (MD) simulations. We find that the orientation of the cyclobis(paraquat-*p*-phenylene) (CBPQT) ring depends dramatically on the coverage, changing in order to obtain highly packed SAMs. The ring lies with its large hollow parallel to the surface at lower coverage (up to one CBPQT per 27 surface Au atoms with a footprint of 1.9 nm^2; **1/27**) when free space is available around it, but as the coverage increases (up to one CBPQT per 12 surface Au atoms with a footprint of 0.9 nm^2; **1/12**), it tilts completely around its axis and lies with its smaller side (paraquat or phenyl ring) parallel to the surface to accommodate the reduced area available. We find that the best packing densities correspond to one CBPQT per 12−18 surface Au atoms (**1/18**−**1/12**) with footprints in the range between 0.9 nm^2 and 1.3 nm^2.

1. Introduction

A most exciting recent development in electronics is the development of molecular components [switches, rectifiers, transistors, interconnects, memories, etc.] suitable for nanomanufacturing of electronic devices as single-molecule junctions or as self-assembled monolayers.[1−7]

Indeed the Stoddart and Heath groups have demonstrated a programmable molecular switch based on a self-assembled monolayer (SAM) of bistable [2]rotaxane (**1**) anchored on polysilicon electrodes with poly(ethylene oxide)-type linkers and covered with a Ti/Al electrode[5] and a SAM of related [2]-catenanes incorporated between a poly-Si[8] or a single-walled carbon nanotube electrode[9] and a Ti/Al electrode. It is thought

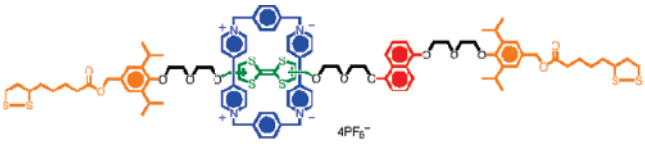

1

that the reversible turning on and off of this switch involves moving the cyclobis(paraquat-*p*-phenylene) (CBPQT^{4+}; blue ring) shuttle between the tetrathiafulvalene (TTF; green station) and the 1,5-dioxynaphthalene (DNP; red station), which is stimulated by oxidation and reduction of the TTF.[10,11] However these mechanistic arguments are based on studies of a solution-based system rather than direct measurement on the solid-state devices.[5,12] Indeed there is little information available on the structure and behavior of **1** on electrode surfaces, especially in solid-state devices.[5,12]

To provide a rational approach to improving and optimizing these devices, we wish to establish the mechanisms underlying the performance of these devices. Consequently we wish to model directly the working switch. However the demonstrated successful rotaxane switch on poly Si has a complex ill-defined electrode structure, with little known about the actual conformation of the molecules on the surfaces or of the pathway for tunneling of the current. This makes this system too complex to analyze and optimize. Consequently we will consider simpler systems in which the rotaxane molecules are anchored onto gold or platinum with disulfide bonds[12] or in which the a [2]catenane is used as the switch.[8,9,13]

Since the switching mechanism (that is the shuttling motion *and* the electrical properties) of **1** depends on its structure on the electrodes, we consider that the first step is to predict the

(1) Carroll, R. L.; Gorman, C. B. *Angew. Chem., Int. Ed.* **2002**, *41*, 4378−4400.
(2) Heath, J. R.; Ratner, M. A. *Physics Today* **2003**, *56*, 43−49.
(3) Reed, M. A.; Tour, J. M. *Sci. Am.* **2000**, *282*, 86−93.
(4) Joachim, C.; Gimzewski, J. K.; Aviram, A. *Nature* **2000**, *408*, 541−548.
(5) Luo, Y.; Collier, C. P.; Jeppesen, J. O.; Nielsen, K. A.; Delonno, E.; Ho, G.; Perkins, J.; Tseng, H.-R.; Yamamoto, T.; Stoddart, J. F.; Heath, J. R. *ChemPhysChem* **2002**, *3*, 519−525.
(6) Collier, C. P.; Wong, E. W.; Belohradsky, M.; Raymo, F. M.; Stoddart, J. F.; Kuekes, P. J.; Williams, R. S.; Heath, J. R. *Science* **1999**, *285*, 391−394.
(7) Wong, E. W.; Collier, C. P.; Behloradsky, M.; Raymo, F. M.; Stoddart, J. F.; Heath, J. R. *J. Am. Chem. Soc.* **2000**, *122*, 5831−5840.
(8) Collier, C. P.; Mattersteig, G.; Wong, E. W.; Luo, Y.; Beverly, K.; Sampaio, J.; Raymo, F. M.; Stoddart, J. F.; Heath, J. R. *Science* **2000**, *289*, 1172−1175.
(9) Diehl, M. R.; Steuerman, D. W.; Tseng, H.-R.; Vignon, S. A.; Star, A.; Celestre, P. C.; Stoddart, J. F.; Heath, J. R. *ChemPhysChem* **2003**, *4*, 1335−1339.
(10) Balzani, V.; Credi, A.; Mattersteig, G.; Matthews, O. A.; Raymo, F. M.; Stoddart, J. F.; Venturi, M.; White, A. J. P.; Williams, D. J. *J. Org. Chem.* **2000**, *65*, 1924−1936.
(11) Tseng, H.-R.; Vignon, S. A.; Stoddart, J. F. *Angew. Chem., Int. Ed.* **2003**, *42*, 1491−1495.
(12) Yu, H.; Luo, Y.; Beverly, K.; Stoddart, J. F.; Tseng, H.-R.; Heath, J. R. *Angew. Chem., Int. Ed.* **2003**, *42*, 5706−5711.
(13) Pease, A. R.; Jeppesen, J. O.; Stoddart, J. F.; Luo, Y.; Collier, C. P.; Heath, J. R. *Acc. Chem. Res.* **2001**, *34*, 433−444.

SAM structure (intermolecular packing as well as intramolecular conformation) of **1** on a gold surface. Given a well-defined structure, we can consider direct tests on the mechanism and interpretation of the conductivity measurements on the Stoddart−Heath solid-state device.

There have been previous theoretical studies on the Stoddart−Heath-type rotaxanes, using both quantum-mechanics (QM)[14−18] and force-field (FF)[19−22] approaches, but the emphasis has been on the isolated rotaxane in a vacuum or in solution. There has been no effort yet to establish its SAM structure on a surface.

1 is a very complicated compound with numerous possible conformations, among which the preference between the "folded" and "unfolded" (between two stations) conformations is the most important to settle.[23,24] Thus we study here the SAM structure of **1** in a "bottom-up" approach. That is, we start with a simpler but essential part of **1**, avoiding the conformation issues interlacing with the SAM packing issue. The first model we examine is **4**, a simpler version of the left half of **1**, the CBPQT shuttle (**2**) on the TTF station anchored to a gold surface through the 1,2-disulfide of thioctate (1,2-dithiolane-3-pentanoate) (**3**). **4** has been synthesized and self-assembled on a gold surface[25,26] and has shown reversible complexation−decomplexation of CBPQT-TTF along with the reduction−oxidation of TTF as assumed for **1**. With this "half" [2]rotaxane, the "folded-versus-unfolded" conformation issue can be separated from the SAM packing issue, which also involves the orientation of the CBPQT ring and the arrangement of PF_6 anions around it for each packing density on a surface. Once the SAM packing issue is established, we can add another half of **1** (DNP station) on top of **4** toward a more complete model on a sounder basis.

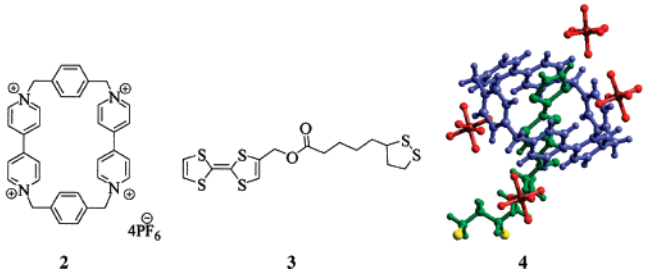

2 **3** **4**

We report molecular dynamics (MD) simulations for various coverages of SAM of **4** on Au(111), while diluting with butanethiolate coadsorbates, a surface diluent, or space-filler used in experiments.[25−27] These studies are then used to determine the optimum packing density of **4** on Au(111) and to establish the coverage-dependence of the SAM structure. This structure can be used as a template on which the whole [2]-rotaxane **1** can be built for future studies.

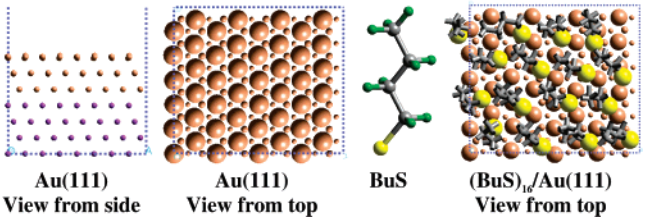

Figure 1. (Left) ($4\sqrt{3} \times 6$) unit cell of Au(111) surface with 48 Au atoms at each layer. This is modeled with a periodic seven-layer slab, of which the bottom four layers were fixed. (Right) SAM with 16 butanethiolates per ($4\sqrt{3} \times 6$) unit cell of Au(111), leading to a coverage of 1/3.

Table 1. Composition of SAM at Various Coverages (θ) of **4**

unit cell	n(Au$_{surf}$)	n(S)[a]	n(**4**)	n(BuS)	θ (**4**/Au$_{surf}$)
$4\sqrt{3} \times 6$	**48**	16	**0**	16	**0 (1/∞)**
$4\sqrt{3} \times 6$	**48**	16	**1**	14	**1/48**
$3\sqrt{3} \times 6$	**36**	12	**1**	10	**1/36**
$3\sqrt{3} \times 9$	**54**	18	**2**	14	**1/27**
$4\sqrt{3} \times 6$	**48**	16	**2**	12	**1/24**
$2\sqrt{3} \times 9$	**36**	12	**2**	8	**1/18**
$2\sqrt{3} \times 12$	**48**	16	**3**	10	**1/16**
$2\sqrt{3} \times 15$	**60**	20	**4**	12	**1/15**
$2\sqrt{3} \times 3$	**12**	4	**1**	2	**1/12**

[a] n(S) (the number of Sanchors) = 2 × n(**4**) + n(BuS).

2. Calculation Details

The Au(111) surface was modeled using a periodic seven-layer slab where the bottom four layers were fixed at its bulk position (*fcc*, r(Au−Au) = 2.884 Å) throughout the study (Figure 1). Different sizes of unit cell were used for different SAM coverages (Table 1). The 48-surface-Au-atom unit cell shown in Figure 1 is denoted ($4\sqrt{3} \times 6$), while ($3\sqrt{3} \times 6$) denotes a 36-surface-Au-atom unit cell and so on.

Butanethiolates (BuS$^{\bullet}$ derived from butanethiols or dibutyl disulfides)[25−27] were introduced to coadsorb with **4** on Au surfaces to control the surface coverage of **4** and to fill the empty space (vacant adsorption sites) at the bottom part of the complex, caused by the size imbalance between the bulky CBPQT ring (7 Å × 11 Å) and the thin TTF-thioctate anchor part. Figure 1 shows the infinite dilution extreme case, where only BuS's are present on the surface. The consensus established so far (but still controversial[28−33]) is that alkylthiols and dialkyl disulfides adsorb on Au(111) as alkylthiolates[34−38] (at least at room tempera-

(14) Zhang, K.-C.; Liu, L.; Mu, T.-W.; Guo, Q.-X. *Chem. Phys. Lett.* **2001**, *333*, 195−198.
(15) Macias, A. T.; Kumar, K. A.; Marchand, A. P.; Evanseck, J. D. *J. Org. Chem.* **2000**, *65*, 2083−2089.
(16) Castro, R.; Berardi, M. J.; Cordova, E.; de Olza, M. O.; Kaifer, A. E.; Evanseck, J. D. *J. Am. Chem. Soc.* **1996**, *118*, 10257−10268.
(17) Jang, Y. H.; Hwang, S.; Kim, Y.-H.; Jang, S. S.; Goddard, W. A., III. *J. Am. Chem. Soc.* **2004**, *126*, 12636−12645.
(18) Deng, W.-Q.; Muller, R. P.; Goddard, W. A., III. *J. Am. Chem. Soc.* **2004**, *126*, 13562−13563.
(19) Grabuleda, X.; Ivanov, P.; Jaime, C. *J. Org. Chem.* **2003**, *68*, 1539−1547.
(20) Kaminski, G. A.; Jorgensen, W. L. *J. Chem. Soc., Perkin Trans. 2* **1999**, 2365−2375.
(21) Grabuleda, X.; Jaime, C. *J. Org. Chem.* **1998**, *63*, 9635−9643.
(22) Zheng, X.; Sohlberg, K. *J. Phys. Chem. A* **2003**, *107*, 1207−1215.
(23) Yamamoto, T.; Tseng, H.-R.; Stoddart, J. F.; Balzani, V.; Credi, A.; Marchioni, F.; Venturi, M. *Collect. Czech. Chem. Commun.* **2003**, *68*, 1488−1514.
(24) Jeppesen, J. O.; Vignon, S. A.; Stoddart, J. F. *Chem.−Eur. J.* **2003**, *9*, 4611−4625.
(25) Cooke, G.; Duclairoir, F. M. A.; Rotello, V. M.; Stoddart, J. F. *Tetrahedron Lett.* **2000**, *41*, 8163−8166.
(26) Bryce, M. R.; Cooke, G.; Duclairoir, F. M. A.; John, P.; Perepichka, D. F.; Polwart, N.; Rotello, V. M.; Stoddart, J. F.; Tseng, H.-R. *J. Mater. Chem.* **2003**, *13*, 2111−2117.
(27) Azehara, H.; Mizutani, W.; Suzuki, Y.; Ishida, T.; Nagawa, Y.; Tokumoto, H.; Hiratani, K. *Langmuir* **2003**, *19*, 2115−2123.
(28) Fenter, P.; Eberhardt, A.; Eisenberger, P. *Science* **1994**, *266*, 1216−1218.
(29) Nishida, N.; Hara, M.; Sasabe, H.; Knoll, W. *Jpn. J. Appl. Phys.* **1996**, *35*, L799−L802.
(30) Nishida, N.; Hara, M.; Sasabe, H.; Knoll, W. *Jpn. J. Appl. Phys.* **1996**, *35*, 5866−5872.
(31) Schonherr, H.; Ringsdorf, H.; Jaschke, M.; Butt, H.-J.; Bamberg, E.; Allinson, H.; Evans, S. D. *Langmuir* **1996**, *12*, 3898−3904.
(32) Ishida, T.; Yamamoto, S.; Mizutani, W.; Motomatsu, M.; Tokumoto, H.; Hokari, H.; Azehara, H.; Fujihira, M. *Langmuir* **1997**, *13*, 3261−3265.
(33) Noh, J.; Hara, M. *Langmuir* **2002**, *18*, 1953−1956.
(34) Nuzzo, R. G.; Zegarski, B. R.; Dubois, L. H. *J. Am. Chem. Soc.* **1987**, *109*, 733−740.
(35) Bain, C. D.; Biebuyck, H. A.; Whitesides, G. M. *Langmuir* **1989**, *5*, 723−727.
(36) Biebuyck, H. A.; Whitesides, G. M. *Langmuir* **1993**, *9*, 1766−1770.
(37) Hagenhoff, B.; Benninghoven, A.; Spinke, J.; Liley, M.; Knoll, W. *Langmuir* **1993**, *9*, 1622−1624.
(38) Noh, J.; Hara, M. *Langmuir* **2000**, *16*, 2045−2048.

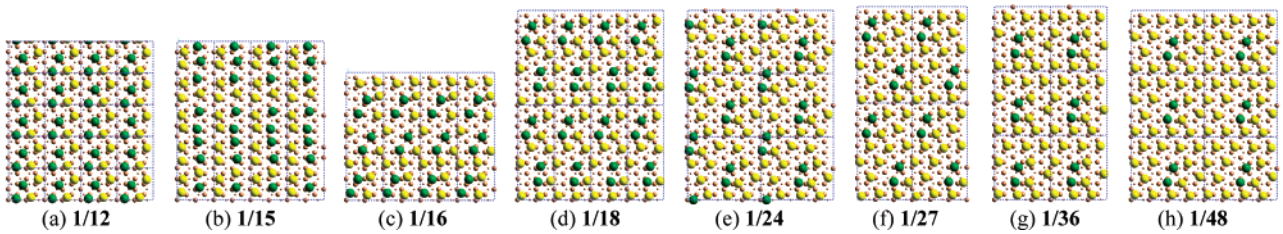

Figure 2. Various coverages for the SAM of **4**. Only Au (light brown) and S anchors (yellow for S from BuS and green for S from **4**) are shown, providing a clear indication of how many BuS's were replaced with **4** for each coverage. These snapshots are for the minimized structures prior to MD simulation.

ture[39,40]) at the coverage of 1/3 at hollow sites[41] (*fcc*[42,43]) or bridge sites[44] or somewhere between them[45−47] in the $(\sqrt{3} \times \sqrt{3})R30°$ configuration[48−50] or in its c(4 × 2) rectangular superlattice[51,52] [= four molecules in $(2\sqrt{3} \times 3)$ lattice]. Thus we introduced 16 BuS onto the *fcc* hollow sites of the 48-surface-Au-atom unit cell of $(4\sqrt{3} \times 6)$ Au(111) surface.

We built eight different finite coverages of uniform SAM of **4** on the top side of the Au(111) surface. The coverages range from a single **4** per 48 surface Au atoms (**1/48**) gradually down to the coverage corresponding to a single **4** per 36 (**1/36**), 27 (**1/27**), 24 (**1/24**), 18 (**1/18**), 16 (**1/16**), 15 (**1/15**), and 12 (**1/12**) surface Au atoms. They correspond to the footprints of 3.46 (**1/48**), 2.59 (**1/36**), 1.94 (**1/27**), 1.73 (**1/24**), 1.30 (**1/18**), 1.15 (**1/16**), 1.08 (**1/15**), and 0.86 nm^2 (**1/12**) per each **4**.

At each coverage we started with the infinitely dilute BuS-only SAM BuS/Au(111) (or its multiples or fractions) and replaced the corresponding number of BuS's with **4**, so that there would be no vacant adsorption site. That is, any adsorption site not occupied by **4** is filled by BuS. Although the coverage of **4** varies from 1/48 to 1/12, the coverage of S is conserved constant (1/3) throughout this study.

Next we must consider how many BuS's are replaced by each **4**. Since it is generally agreed that the disulfide (S−S) bond dissociates on Au surfaces to make two S−Au bonds[34−38] (at least at room temperature[39,40]), we assumed that the S−S bond in the cyclic 1,2-dithiolane of the thioctic anchor is broken to make two S−Au bonds. (This is confirmed with QM calculations that will be reported separately.) The separation between the two S's in its most probable conformation of 1,2-dithiolane after the S−S cleavage ($^{\bullet}SCH_2CH_2CH_2S^{\bullet}$) is around 4.5 Å, which is close to the distance (5.0 Å) between two adjacent adsorption sites of Au(111) in the $(\sqrt{3} \times \sqrt{3})R30°$ SAM of alkanethiolates. The SAM formed by thioctic acids (the bottom of **3** before the condensation reaction with TTF) has been determined to saturate at a coverage of 0.54 nm^2 and 0.47 nm^2.[53,54] more than twice the SAM coverage of 0.216 nm^2 for alkanethiolate on Au(111). Thus, it is likely that each **4** occupies two adsorption sites of Au(111) (that is, six surface Au atoms), and we replaced two BuS's for each **4**.

The compositions of various coverages of SAM are summarized in Table 1 and Figure 2. For example, the $(4\sqrt{3} \times 6)$ unit cell has 48 surface Au atoms covered by a total of 16 S's, so that **1/48** coverage has two S's come from a single **4** with the remaining 14 S's coming from 14 BuS's.

We consider the optimum coverage to have the maximum packing energy (per area; energy density). The packing energy per S (the number of S anchors per area is conserved throughout the study) is defined as

$$\Delta E_{\text{pack}} = \frac{1}{2m+n}\{E[\text{SAM/Au}] - E[\text{Au}] - mE[\mathbf{4}(\text{g})] - nE[\text{BuS(g)}]\} \quad (1)$$

The energy (E) of each system (and other properties), either on surface or in the gas phase, was estimated at 298 K from the 1-ns NVT MD simulations using *Cerius2*.[55]

The FF for Au was developed to reproduce its bulk properties (density, lattice energy, and heat capacity).[56] The FF between S and Au was developed to reproduce the QM binding energy and geometry of an ethanethiolate or fluoroethanethiolate on Au_8 or Au_{32} clusters.[56] The Dreiding FF[57] was used otherwise for BuS, TTF-thioctate, CBPQT, and PF_6, except that since PF_6 is octahedral we used a cosine (cos 4θ) angle bending function (with minima at multiples of 90°).

For the Coulombic part of the FF, the atomic charge of each Au atom was fixed at zero throughout the study, while the atomic charges of each component ($^2BuS^{\bullet}$, TTF-thioctate, $CBPQT^{4+}$, and PF_6^-) were calculated separately from QM (Mulliken) after full geometry optimization at the level of B3LYP[58−62]/6-31G** in the gas phase, using *Jaguar* v4.2.[63] We did not take into account additional charge polarization or adsorbate−substrate charge transfer. (We included such charge-transfer effects in other simulations and found no significant effects.[56])

We found that 1-ns NPT MD simulations using this FF reproduced within 5% the densities of crystals containing $CBPQT^{4+}$ (or PQT^{2+}, a fraction of CBPQT), PF_6^- and TTF units (at corresponding

(39) Kluth, G. J.; Carraro, C.; Maboudian, R. *Phys. Rev. B* **1999**, *59*, R10449−R10452.
(40) Kato, H. S.; Noh, J.; Hara, M.; Kawai, M. *J. Phys. Chem. B* **2002**, *106*, 9655−9658.
(41) Sellers, H.; Ulman, A.; Shnidman, Y.; Eilers, J. E. *J. Am. Chem. Soc.* **1993**, *115*, 9389−9401.
(42) Groenbeck, H.; Curioni, A.; Andreoni, W. *J. Am. Chem. Soc.* **2000**, *122*, 3839−3842.
(43) Yourdshahyan, Y.; Zhang, H. K.; Rappe, A. M. *Phys. Rev. B* **2001**, *63*, 081405.
(44) Vargas, M. C.; Giannozzi, P.; Selloni, A.; Scoles, G. *J. Phys. Chem. B* **2001**, *105*, 9509−9513.
(45) Hayashi, T.; Morikawa, Y.; Nozoye, H. *J. Chem. Phys.* **2001**, *114*, 7615−7621.
(46) Gottschalck, J.; Hammer, B. *J. Chem. Phys.* **2002**, *116*, 784−790.
(47) Akinaga, Y.; Nakajima, T.; Hirao, K. *J. Chem. Phys.* **2001**, *114*, 8555−8564.
(48) Widrig, C. A.; Alves, C. A.; Porter, M. D. *J. Am. Chem. Soc.* **1991**, *113*, 2805−2810.
(49) Chidsey, C. E. D.; Loiacono, D. N. *Langmuir* **1990**, *6*, 682−691.
(50) Strong, L.; Whitesides, G. M. *Langmuir* **1988**, *4*, 546−558.
(51) Camillone, N., III; Chidsey, C. E. D.; Liu, G.; Scoles, G. *J. Chem. Phys.* **1993**, *98*, 3503−3511.
(52) Poirier, G. E.; Tarlov, M. J. *Langmuir* **1994**, *10*, 2853−2856.
(53) Wang, Y.; Kaifer, A. E. *J. Phys. Chem. B* **1998**, *102*, 9922−9927.
(54) Madoz, J.; Kuznetzov, B. A.; Medrano, F. J.; Garcia, J. L.; Fernandez, V. M. *J. Am. Chem. Soc.* **1997**, *119*, 1043−1051.
(55) *Cerius2*, v4.0; Molecular Simulations, Inc.: 1999.
(56) Jang, S. S.; Jang, Y. H.; Kim, Y.-H.; Goddard, W. A., III; Flood, A. H.; Laursen, B. W.; Tseng, H.-R.; Stoddart, J. F.; Jeppeson, J. O.; Choi, J. W.; Steuerman, D. W.; Delonno, E.; Heath, J. R. *J. Am. Chem. Soc.* **2005**, *127*, 1563−1575.
(57) Mayo, S. L.; Olafson, B. D.; Goddard, W. A., III. *J. Phys. Chem.* **1990**, *94*, 8897−8909.
(58) Slater, J. C. *Quantum Theory of Molecules and Solids. Vol. 4. The Self-Consistent Field for Molecules and Solids*; McGraw-Hill: New York, 1974.
(59) Becke, A. D. *Phys. Rev. A* **1988**, *38*, 3098−3100.
(60) Vosko, S. H.; Wilk, L.; Nusair, M. *Can. J. Phys.* **1980**, *58*, 1200−1211.
(61) Lee, C.; Yang, W.; Parr, R. G. *Phys. Rev. B* **1988**, *37*, 785−789.
(62) Miehlich, B.; Savin, A.; Stoll, H.; Preuss, H. *Chem. Phys. Lett.* **1989**, *157*, 200−206.
(63) *Jaguar 4.2*; Schrodinger Inc.: Portland, OR, 2000.
(64) Odell, B.; Reddington, M. V.; Slawin, A. M. Z.; Spencer, N.; Stoddart, J. F.; Williams, D. J. *Angew. Chem., Int. Ed. Engl.* **1988**, *27*, 1547−1550.
(65) Anelli, P. L.; Ashton, P. R.; Ballardini, R.; Balzani, V.; Delgado, M.; Gandolfi, M. T.; Goodnow, T. T.; Kaifer, A. E.; Philp, D.; Pietraszkiewicz, M.; Prodi, L.; Reddington, M. V.; Slawin, A. M. Z.; Spencer, N.; Stoddart, J. F.; Vicent, C.; Williams, D. J. *J. Am. Chem. Soc.* **1992**, *114*, 193−218.
(66) Philp, D.; Slawin, A. M. Z.; Spencer, N.; Stoddart, J. F.; Williams, D. J. *J. Chem. Soc., Chem. Commun.* **1991**, 1584−1586.

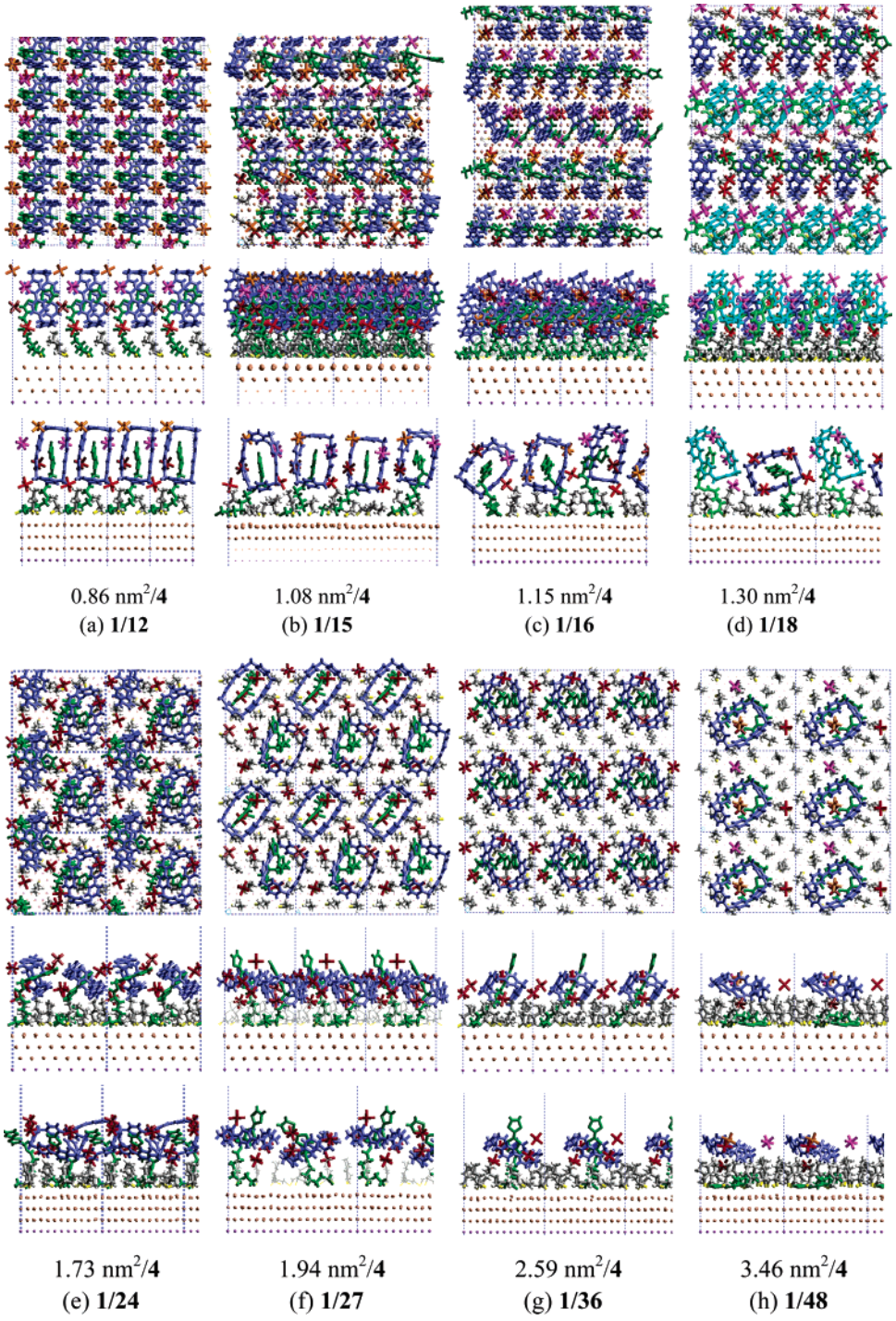

Figure 3. SAM structure and footprints of **4** for various coverages. Most snapshots are after 1-ns MD simulations. Blue (CBPQT), green (TTF), gray (BuS), pink/orange (PF_6). (Top) View along *z*-axis (surface normal), (middle) view along *y*, (bottom) view along *x*.

temperatures)[64−67] and led to a good value for the binding energy between $(CBPQT)(PF_6)_4$ and TTF.[13,68,69] The atomic charges, FF parameters, and FF validation results are available in the Supporting Information.

3. Results

The SAM structures at eight different coverages are shown together in Figure 3. The packing energy and the orientation of the CBPQT ring (defined as the orientation of the longest moment-of-inertia vector with respect to the *x*-axis, the surface normal) of those SAMs are summarized in Figure 4 and Tables 2−3. These MD simulations indicate that the optimum packing (in a vacuum) of **1/15** leads to a 1.08 nm^2 footprint per **4**. This is a surprisingly high density for the SAM of **4** on Au(111), since the conventional view is that the CBPQT ring encircles

(67) Cooke, G.; de Cremiers, H. A.; Duclairoir, F. M. A.; Gray, M.; Vaqueiro, P.; Powell, A. V.; Rosair, G.; Rotello, V. M. *Tetrahedron Lett.* **2001**, *42*, 5089−5091.
(68) Anelli, P.-L.; Asakawa, M.; Ashton, P. R.; Bissell, R. A.; Clavier, G.; Gorski, R.; Kaifer, A. E.; Langford, S. J.; Mattersteig, G.; Menzer, S.; Philp, D.; Slawin, A. M. Z.; Spencer, N.; Stoddart, J. F.; Tolley, M. S.; Williams, D. J. *Chem.—Eur. J.* **1997**, *3*, 1113−1135.
(69) Bryce, M. R.; Cooke, G.; Duclairoir, F. M. A.; Rotello, V. M. *Tetrahedron Lett.* **2001**, *42*, 1143−1145.

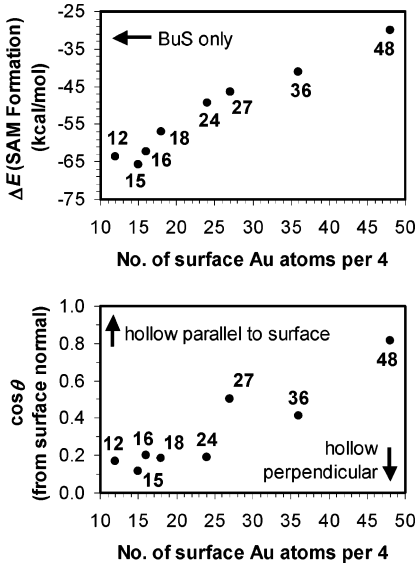

Figure 4. Coverage-dependent packing energy and ring orientation of **4** from 1-ns NVT MD simulations at 298 K (see Tables 2 and 3 for detailed numbers). The ring orientation (θ from the *z*-axis, the surface normal) is represented by the average *z*-component of the longest component of the moment-of-inertia vector of the CBPQT ring component of **4**.

Table 2. Coverage-Dependent SAM-Packing Properties of **4**[a]

coverage[b] n(**4**)/n(Au$_{surf}$)	ΔE_{pack}(/S) (kcal/mol)	stress(x) (GPa)	stress(y) (GPa)
0 (1/∞)	−31.8 ± 0.4	0.053	0.045
1/48	−38.2 ± 0.5	0.078	0.090
1/36	−41.2 ± 0.4	0.049	0.057
1/27	−46.5 ± 0.3	0.042	0.005
1/24	−49.3 ± 0.4	−0.001	−0.007
1/18	−57.0 ± 0.4	0.03	−0.01
1/16	−62.3 ± 0.4	0.042	0.04
1/15	−65.7 ± 0.3	0.14	0.11
1/12	−63.7 ± 0.4	0.49	0.73

[a] From 1-ns MD simulations at 298 K. The averages were taken after equilibration (which varied from 0 to 400 ps), and the standard deviations were estimated from the six to ten 100-ps block averages over the sampling periods. As shown in Figure 5, the **1/48** case leads to decomplexation of **4** after the first three blocks (300 ps) of simulation, so only this region was used for estimating the packing energy. For the uncomplexed state, we find a packing energy of −42.6 ± 0.4 kcal/mol, averaged over last 600 ps. [b] The 48-atom surface unit cell has an area of 3.46 nm^2 so that the optimum coverage (**1/15**) is 1.08 nm^2/**4**.

Table 3. Coverage-Dependence of Ring Orientation of **4**[a]

coverage [n(**4**)/n(Au$_{surf}$)]	cos θ	θ (deg)
1/48	0.81 ± 0.05	35 ± 5
1/36	0.41 ± 0.07	65 ± 4
1/27	0.50 ± 0.09	60 ± 6
1/24	0.19 ± 0.12	79 ± 7
1/18	0.19 ± 0.13	79 ± 8
1/16	0.20 ± 0.11	78 ± 7
1/15	0.12 ± 0.12	83 ± 7
1/12	0.17 ± 0.03	80 ± 2

[a] The angle between the longest principal axis of the CBPQT ring (which represents the normal vector to the hollow of CBPQT) and the surface normal of Au(111). The averages and standard deviations were estimated over 100 snapshots taken every 10 ps over the entire 1-ns MD simulations.

one of the stations of the fully extended [2]rotaxane **1**. Such a structure would require spacings of at least 13 Å × 9 Å center-to-center (including vdW radii) and most likely more because of the Coulombic repulsion between the four positive charges

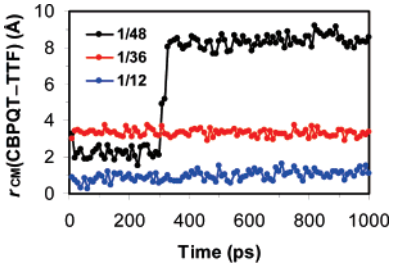

Figure 5. CM(center of mass)-to-CM distances between the CBPQT ring and TTF for three coverages (**1/48**, **1/36**, and **1/12**), which were taken every 10 ps over the 1-ns MD simulations. The big jump in the **1/48** case after 300 ps indicates that the TTF has slipped from the CBPQT ring.

lying parallel to the electrode surface. This would require at least 1.73 nm^2 per CBPQT. However, we find that for the more congested coverages, the CBPQT ring reorients with respect to the surface-parallel axes, so that it occupies a smaller surface area by lying on one of its sides (smaller paraquat ring or even smaller phenyl ring) parallel to the surface.

Ring Parallel to the Surface and Decomplexed (1/48). This has a footprint of 3.45 nm^2 per **4** (one **4** per 48 surface gold atoms in the $4\sqrt{3} \times 6$ unit cell). This provides room for the CBPQT ring to sit on the surface with its large hollow parallel to the surface, which is able to move on the surface. This latter motion allows the CBPQT to decomplex from the TTF at ∼300 ps, as indicated by the abrupt jump in the CM(center of mass)-to-CM distance between the CBPQT ring and TTF from 2.2 ± 0.3 Å (over 0 to 300 ps) to 8.4 ± 0.3 Å (over 400 to 1000 ps) (Figure 5).

Ring Parallel to the Surface (1/36 and 1/27). The SAM was squeezed to three-quarters in the *x*-direction (one **4** per 36 surface gold atoms in a $3\sqrt{3} \times 6$ unit cell; **1/36**) and then in the *y* direction (two **4**s per 54 surface gold atoms in a $3\sqrt{3} \times 9$ unit cell; **1/27**). With footprints of 2.59 and 1.94 nm^2 per **4**, these SAMs have room enough for the CBPQT ring to sit on the surface with its large hollow parallel to the surface but not enough to move around on the surface. The CBPQT and TTF stay as complexed throughout the 1-ns simulations.

Ring Tilts around the *y*-Axis (1/24). On the other hand, squeezing the **1/48** SAM in both the *x*- and *y*-directions by inserting one more **4** into the original unit cell (now two **4**'s in a $4\sqrt{3} \times 6$ unit cell; **1/24**), the "lying-down" orientation which requires a footprint of 1.73 nm^2 per CBPQT ring no longer fits, especially in the *x*-direction, with the result that they start to tilt with respect to the *y*-axis in order to relax the surface pressure in the *x*-direction. The PF_6^- anions locate between the four positively charged ring faces (the edge of the hollow) to achieve the most favorable electrostatic interaction.

Ring Tilted upright around *y*-Axis (1/18). The **1/27** SAM was further squeezed to two-thirds in the *x*-direction (two **4**'s per 36 surface gold atoms in a $2\sqrt{3} \times 9$ unit cell; leading to a footprint of 1.30 nm^2 per **4**). Indeed each CBPQT now tilts with respect to its *y*-axis completely to the upright orientation with their narrow sides (paraquat or phenyl rings) parallel the surface.

Ring Rotating around *x*-Axis (1/16, 1/15, and 1/12). The **1/18** SAM was further squeezed now in the *y*-direction to the following:

(1) **1/16** (three **4**'s per 48 surface gold atoms in the $2\sqrt{3} \times 12$ unit cell; 1.15 nm^2 footprint per **4**),

(2) **1/15** (four **4**'s per 60 surface gold atoms in the $2\sqrt{3} \times 15$ unit cell; 1.08 nm^2 footprint per **4**), and

(3) **1/12** (one **4** per 12 surface gold atoms in the $2\sqrt{3} \times 3$ unit cell; 0.86 nm^2 footprint per **4**).

This shows a gradual tilting of the CBPQT ring around the *x*-axis and by **1/12** coverage the complete tilt to the upright orientation with the phenyl ring parallel to the surface. However, by **1/12** the SAM packing energy starts decreasing and the surface-parallel component of the stress increases abruptly. Thus this **1/12** SAM (0.83 nm^2 footprint) is the upper limit of the packing density for a single layer SAM.

Unfortunately there is little in the way of experimental results on the SAMs of **1** or **4** with which to compare our simulation results. This is surprising because such studies could provide unambiguous information valuable for understanding the more complex rotaxane- and catenane-based devices, and we strongly urge the experimentalists to test some of our predictions.

Even for the simpler SAM of **3** (i.e., TTF-thioctate itself without the CBPQT ring), the coverage reported experimentally on Au surfaces varies from footprints of 0.75 nm^2 (bulkier derivative of **3**),[70] 0.802 nm^2 (TTF-hexadecanethiol),[71] 1.04 nm^2 (TTF-tetrapropanethiol),[72] 1.2 nm^2 (ferrocene-thioctate),[73] up to 1.5 nm^2 (**3**),[74] all of which have much larger footprints than the 0.466 nm^2 based on the size of TTF[71] or the 0.432 nm^2 (twice the typical footprint of alkanethiolate) covered by two S anchors forming two S−Au bonds in the $(\sqrt{3} \times \sqrt{3})R30°$ configuration. This might be due to the instability of the **3**-type SAMs,[70,71,75] unlike the quite stable thioctic acid SAMs.[53,54,76] But it also could indicate that the cathodic-wave current integration method to determine thiolate surface coverages on gold is unreliable.[53,74]

4. Discussion

The more stable higher-coverage SAMs have the paraquat or phenyl ring lying parallel to the surface leading to possible $\pi-\pi$ stacking configuration between stations. This favors increased π-electron transfer through the ring, leading to lower resistance. It might also provide ways to modulate the current by mechanical or acoustical coupling to the SAM.

To illustrate the implications of the structures found at the higher coverages in Figure 3 for the case of the full [2]rotaxane **1**, we added DNP stations through an ethylene oxide linker on top of the SAM structures in Figure 3 to form the structures in Figure 6. Indeed the simulations lead to folded and $\pi-\pi$ stacked conformations where DNP stations sit on (or between) the paraquat or phenyl planes of nearby CBPQT-TTF stations, and the arrangements of those π-stack components (DNP−CBPQT-TTF) seem quite similar to those found in [2]catenanes. Much more complicated situations can also be envisioned in which there are alternative positions of the CBPQT ring, one on the TTF station and the other right next to it on the DNP station.

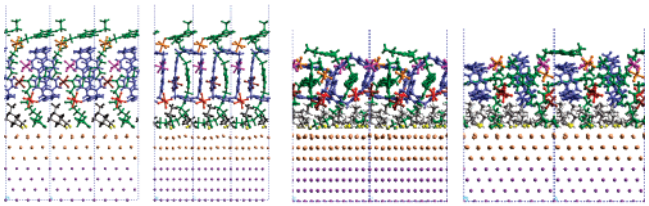

Figure 6. SAM structure and footprint of **4**−$CH_2(OCH_2CH_2)_2$−DNP after 1-ns MD simulations.

This could permit a particularly high coverage. Indeed, in this case the transition between them could be thought of as a phase transition. Indeed a recent Langmuir isotherm measurement of a close relative of **1** indicates an apparent phase transition at a footprint of ~0.9 nm^2, which might be related to such a structural change.

We must point out here that our studies do not yet consider the role of trace amounts of water, which are likely to be important in stabilizing the charged $CBPQT^{4+}$ and PF_6^- groups. This can affect both the energetics and the ease with which the structures can transform with temperature, pressure, and applied voltage. Similarly traces of acetonitrile solvent are likely and might play a role in determining the SAM structure and density. We plan to investigate such effects.

Summarizing, we used MD simulations at 298 K to investigate the SAM structure of the TTF-side half of the Stoddart−Heath type [2]rotaxane on Au(111) surface. We find that the orientation of the CBPQT ring depends dramatically on the coverage, changing to obtain highly packed SAMs. The ring lies with its large hollow parallel to the surface at lower coverage (up to one CBPQT per 27 surface Au atoms with a footprint of 1.9 nm^2; **1/27**) when free space is available around it, but as the coverage increases (up to one CBPQT per 12 surface Au atoms with a footprint of 0.9 nm^2; **1/12**), it tilts completely around its axis and lies with its smaller side (paraquat or phenyl ring) parallel to the surface to accommodate the reduced area available. We find that the best packing densities correspond to one CBPQT per 12−18 surface Au atoms (**1/18**−**1/12**) with footprints in the range between 0.9 nm^2 and 1.3 nm^2. Connecting the DNP half of the real [2]rotaxane to the TTF via an ethylene oxide linkage might lead to slightly different optimum packing densities. We will report separately studies on the SAM of this full [2]rotaxane using MD simulation for both the vacuum and in solution. In addition we are calculating the QM conductivity through the $\pi-\pi$ stack.

Acknowledgment. We thank Prof. J. Fraser Stoddart, Dr. Hsian-Rong Tseng, Dr. Amar Flood, and Dr. Bo W. Laursen at UCLA and Prof. James Heath of Caltech for helpful discussions. This work was initiated with support by the National Science Foundation [NIRT] and continued with support from MARCO-FENA. In addition, the facilities of the MSC were supported by ONR-DURIP, ARO-DURIP, NSF-MRI, and IBM (SUR Grant).

Supporting Information Available: The FF parameters and the FF validation results. This material is available free of charge via the Internet at http://pubs.acs.org.

JA044762W

(70) Liu, H.; Liu, S.; Echegoyen, L. *Chem. Commun.* **1999**, 1493−1494.
(71) Yip, C. M.; Ward, M. D. *Langmuir* **1994**, *10*, 549−556.
(72) Fujihara, H.; Nakai, H.; Yoshihara, M.; Maeshima, T. *Chem. Commun.* **1999**, 737−738.
(73) Tsutsumi, H.; Furumoto, S.; Morita, M.; Matsuda, Y. *J. Electrochem. Soc.* **1992**, *139*, 1522−1525.
(74) Herranz, M. A.; Yu, L.; Martin, N.; Echegoyen, L. *J. Org. Chem.* **2003**, *68*, 8379−8385.
(75) Moore, A. J.; Goldenberg, L. M.; Bryce, M. R.; Petty, M. C.; Moloney, J.; Howard, J. A. K.; Joyce, M. J.; Port, S. N. *J. Org. Chem.* **2000**, *65*, 8269−8276.
(76) Cheng, Q.; Brajter-Toth, A. *Anal. Chem.* **1995**, *67*, 2767−2775.